The Astrophysical Journal, 615:315–322, 2004 November 1

OBSERVATIONS OF THE DIFFUSE FAR-ULTRAVIOLET BACKGROUND WITH THE *FAR ULTRAVIOLET SPECTROSCOPIC EXPLORER*[1]

Jayant Murthy
The Indian Institute of Astrophysics, Koramangala, Bangalore 560 034, India; jmurthy@yahoo.com

and

David. J. Sahnow
Department of Physics and Astronomy, The Johns Hopkins University, Baltimore, MD 21218; sahnow@pha.jhu.edu
Received 2004 May 31; accepted 2004 July 13

ABSTRACT

We have used observations taken under the *Far Ultraviolet Spectroscopic Explorer* (*FUSE*) S405/505 channel realignment program to explore the diffuse far-ultraviolet (FUV; 1000–1200 Å) radiation field. Of the 71 independent locations in that program, we have observed a diffuse signal in 32, ranging in brightness from 1600 to a maximum of 2.9×10^5 photons cm^{-2} sr^{-1} s^{-1} Å^{-1} in Orion. The *FUSE* data confirm that the diffuse FUV sky is patchy with regions of intense emission, usually near bright stars, but also with dark regions, even at low Galactic latitudes. We find a weak correlation between the FUV flux and the 100 μm ratio but with wide variations, perhaps due to differences in the local radiation field.

Subject headings: dust, extinction — ultraviolet: ISM

Online material: color figure

1. INTRODUCTION

The diffuse background from the ultraviolet (UV) to the infrared (IR) is an important tracer of the interstellar dust, and most of our knowledge of the large-scale distribution of the dust has come from missions such as *IRAS* and *COBE* (see, e.g., Sodroski et al. 1997). Scattering in the UV is complementary to the IR emission, and the combination of the two can lead to a unique determination of the interstellar dust parameters. Unfortunately, there have been few observations of the diffuse UV radiation field, and those have been, to a large degree, controversial, as indicated by the conflicting reviews by Bowyer (1991) and Henry (1991). In the far-ultraviolet (FUV; below 1200 Å) band, which we address in this paper, the only significant body of observations comes from Murthy et al. (1999). They used the ultraviolet spectrographs (UVS) aboard the two *Voyager* spacecraft, finding that the FUV sky was very patchy with both dark and bright regions.

In this work, we have used serendipitous observations from the *Far Ultraviolet Spectrographic Explorer* (*FUSE*) under the S405/505 program to further probe the diffuse FUV sky. Although *FUSE* cannot match the sensitivity of the *Voyager* UVS for observations of diffuse sources because of its relatively small field of view, we have, nevertheless, found many locations that do indeed have a strong enough signal to be detected by *FUSE*. We concentrate here on presenting the overall results from our study and will discuss individual locations in detail in subsequent papers.

2. OBSERVATIONS AND DATA ANALYSIS

The *FUSE* spacecraft and mission has been described by Moos et al. (2000) and by Sahnow et al. (2000). The instrument consists of four co-aligned optical channels, two of which are coated with silicon carbide (SiC) and two with lithium fluoride (LiF) over aluminum, providing coverage over the spectral range from 905 to 1187 Å. Observations may be made through any of three apertures: the LWRS ($30'' \times 30''$) aperture, the MDRS ($4'' \times 20''$) aperture, and the HIRS ($1\farcs25 \times 20''$) aperture. In principle, extended radiation will be visible in all four channels and through all the apertures but, in practice, only the brightest sources can be detected in any other than the LiF LWRS channel. *FUSE* was launched on 1999 June 24 into a low Earth orbit by a Delta II rocket and has been observing astronomical targets, mostly point sources, since then.

The S405/505 program is intended to allow the *FUSE* spectrographs to thermalize prior to a channel realignment. As such, these pointings are generally observations of blank sky near one of a number of alignment stars with exposure times on the order of a few thousand seconds. The complete list of pointings is available from the MAST archive at STScI,[2] and, of those, we have examined all that were available before 2003 September 1. We downloaded the raw data and processed them using the standard CalFUSE pipeline (ver. 2.4; Dixon et al. 2002) with two major modifications.

The standard *FUSE* observation consists of a number of different exposures including both the "DAY" and the "NIGHT" part of the orbit. Because of the faintness of the diffuse background, we used only the "NIGHT" photons, thereby eliminating most of the airglow lines other than the Lyman lines of atmospheric hydrogen. There may still be residual amounts of the O I lines around 1040 Å and the N I lines at 1134 Å, but these are generally weak and will not be significant contributors to the continuum emission reported on here (Feldman et al. 2001). Finally, we combined the different exposures (using the program *ttag_combine.c* available as part of the standard *FUSE* distribution).

We have found that the standard background subtraction considerably overestimates the instrumental background for the faint extended sources observed in this program and so,

[1] Based on observations made with the NASA-CNES-CSA *Far Ultraviolet Spectroscopic Explorer*. *FUSE* is operated for NASA by The Johns Hopkins University under NASA contract NAS5-32985.

[2] See http://archive.stsci.edu.

TABLE 1
BANDS USED FOR BACKGROUND EXTRACTION

Number	Detector	Columns	Wavelengths (Å)
1	LiF 1A	1100–6000	987.08–1020.77
2	LiF 1A	7500–15,000	1034.84–1081.37
3	LiF 1B	2000–7000	1100.28–1133.69
4	LiF 1B	7000–14,000	1133.69–1180.07
5	LiF 2A	2000–7000	1175.32–1141.97
6	LiF 2A	9000–14,000	1128.57–1095.03

instead, empirically estimated the background from the counts in the detector just off the aperture and subtracted that from the spectrum. In most of the targets in this program, the signal was too faint to obtain a useful spectrum even though a diffuse continuum was clearly apparent to the eye. We therefore used the *ttgd* image of the detector plane (step 19 from the CalFUSE Pipeline Reference Guide; Dixon et al. 2002) and integrated over bands selected to avoid the airglow lines (Table 1). This is illustrated in Figure 1, where we have shown an image of one of the detector segments (1A) for the S4050201 observation. The two bands (rows [1] and [2]) of Table 1 are shown as large boxes on either side of the LiF LWRS Lyβ feature.

The enhancement due to the diffuse continuum is readily visible in the LiF LWRS aperture, and, upon integration over the bands, all the apertures stand out over the background. This is clearly shown in Figure 1, where we have superimposed a cut across the image in which the data have been collapsed in the spectral direction over the right-hand box of the figure (cols. 7500–15,000 from row [2] of Table 1). Although in principle a diffuse signal will be visible in all the apertures, we have used only the data from the LiF LWRS aperture because its throughput is so much greater than the others. Similarly, the data from the 2B detector do not add any value to the diffuse sky determination because of its much lower sensitivity.

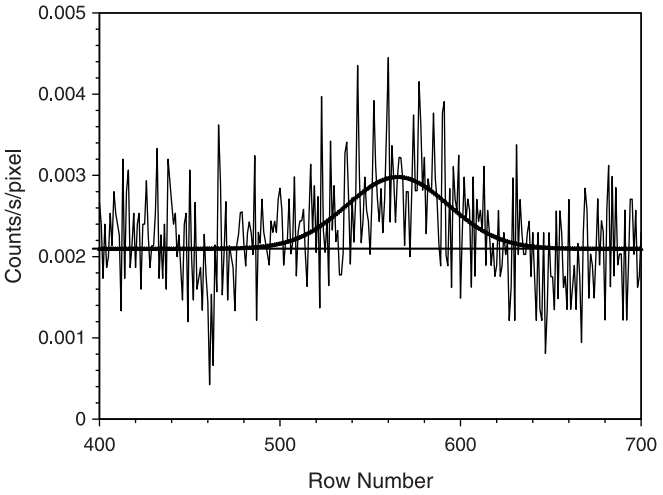

FIG. 2.—Cut through the detector plane from S4050201 (Fig. 1). We have integrated between columns 7500 and 15,000 (row [2] of Table 1), which avoids the Lyβ airglow lines. The LiF LWRS aperture stands out clearly above the background, and we have fit the signal with a Gaussian, shown as a thick line. As mentioned above, the level of emission here is 3300 $\pm$ 1400 photons cm^{-2} sr^{-1} s^{-1} Å^{-1}. The noise level in the data sets a detection limit on the order of 2000 photons cm^{-2} sr^{-1} s^{-1} Å^{-1}.

As we have seen from Figure 1, the emission in the LiF LWRS aperture in particular stands out from the background, and we have replotted the signal in the immediate neighborhood of the aperture in Figure 2. We have then fitted this profile with a Gaussian (plus a background) with uncertainties defined by the rms deviations adjacent to the aperture and found 90% confidence limits on the level of the diffuse background using the procedure of Lampton et al. (1976). Those targets in which

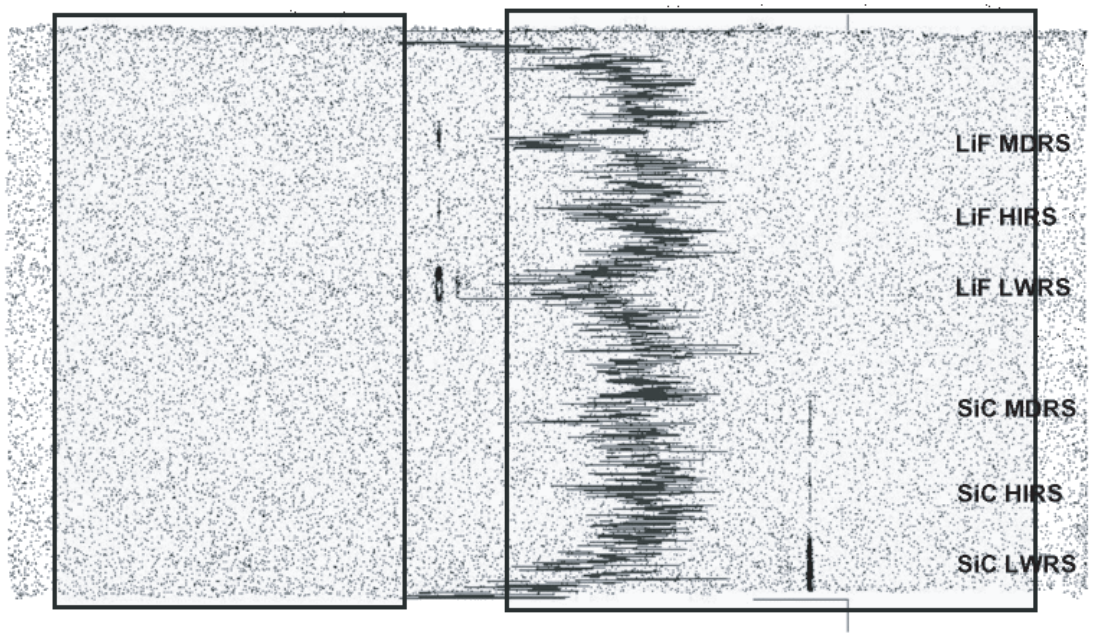

FIG. 1.—Image of the 1A detector segment from S4050201, a 5626 s observation of blank sky offset by 90″ from a white dwarf. The LiF apertures are imaged onto the top half of the image and the SiC onto the bottom half with the strong terrestrial Lyβ line seen as the strongest line in each of the six apertures. The image scale can be derived from the sides of the boxes, which are at column numbers 1100, 6000, 7500, and 15,000 from left to right. Superimposed on the image is a cut across the image with the data collapsed in the spectral direction over one of the wavelength bands (cols. 7500–15,000; see Table 1) in which the enhancements due to the diffuse signal in the different apertures can be clearly seen. Note that the defined bands (shown by the two large boxes) exclude the strong geocoronal emission lines seen in the image. A detailed analysis (see below) shows that the emission has a flux of 3300 $\pm$ 1400 photons cm^{-2} sr^{-1} s^{-1} Å^{-1} at a 90% confidence level and a mean wavelength of 1058 Å. The rise in signal at the top and bottom of the active area is due to edge effects in the microchannel plates.

TABLE 2

POSITIVE DETECTIONS OF DIFFUSE RADIATION

Data Set	Target	R.A. (deg)	Decl. (deg)	l (deg)	b (deg)	Time (s)	1	2	3	4	5	6
S40502/01	WD 0439+466	70.8	46.7	158.5	0.5	5626	7735 ± 4498	3316 ± 1377	3194 ± 1594	3455 ± 1708	2887 ± 1311	3200 ± 2182
S40506/01	HD 093840	162.3	−46.8	282.1	11.1	12,998	4850 ± 3846	2088 ± 751	2039 ± 1063	3429 ± 1531	1196 ± 958	2860 ± 2444
S40507/01	HD 96548	166.6	−65.7	292.3	−60.8	7843	13,639 ± 5393	7051 ± 1011	9408 ± 2007	9441 ± 2200	8141 ± 1694	8979 ± 1515
S40514/01	HD 163522	269.7	−42.5	349.6	−9.1	11,001	2891 ± 1606	3034 ± 838	3356 ± 896	4910 ± 1211	3269 ± 1610	2977 ± 1088
S40515/01	HD 92809	160.4	−58.8	286.8	−0.0	11,303	9425 ± 2358	10,351 ± 616	18,414 ± 1315	23,184 ± 1752	20,241 ± 1468	17,343 ± 1152
S40515/02	HD 92809	160.4	−58.8	286.8	−0.0	3542	11,878 ± 5296	10,283 ± 1276	18,356 ± 2534	22,032 ± 2588	19,354 ± 2321	20,185 ± 2779
S40517/01	HD 104994	181.3	−62.1	297.6	0.3	4154	18,358 ± 3483	12,452 ± 1006	14,601 ± 1866	15,959 ± 2801	16,094 ± 2380	15,623 ± 1615
S40520/01	HD 153426	255.3	−38.2	347.1	2.4	7521	14,672 ± 3371	12,548 ± 959	17,809 ± 1621	22,077 ± 2269	19,387 ± 1643	16,278 ± 1466
S40521/01	BD +28D4211	327.8	28.9	81.9	−19.3	10,730	6525 ± 2248	3529 ± 747	2695 ± 887	3675 ± 1558	2970 ± 2503	1549 ± 821
S40522/01	HD 216438	343.0	53.7	105.7	−5.1	3971	1973 ± 1973	1846 ± 730	1174 ± 838	5287 ± 1991	4156 ± 3067	3309 ± 2832
S40526/01	HD 156385	259.9	−45.6	343.2	−4.8	7029	3925 ± 3925	3328 ± 1148	6065 ± 1399	8176 ± 2220	6189 ± 1965	3860 ± 1557
S40527/01	Sk 71D45	82.8	−71.1	281.9	−32.0	6754	21,096 ± 2700	17,857 ± 858	21,757 ± 1638	26,638 ± 2449	25,196 ± 2106	23,063 ± 1509
S40527/02	Sk 71D45	82.8	−71.1	281.9	−32.0	3893	23,156 ± 3259	19,405 ± 1085	21,430 ± 2226	26,891 ± 2548	25,993 ± 2332	23,756 ± 1747
S40528/01	HD 187459	297.2	33.4	68.8	3.9	5129	4100 ± 4100	3298 ± 1810	4949 ± 1376	6359 ± 2227	5502 ± 2025	4567 ± 1510
S40529/01	HD 013268	32.9	56.2	134.0	−5.0	6730	3840 ± 3840	2347 ± 1081	2241 ± 1134	2540 ± 2017	2340 ± 1102	2825 ± 2282
S40529/02	HD 013268	32.9	56.2	134.0	−5.0	5113	3955 ± 3955	1949 ± 1254	2980 ± 1264	4374 ± 2033	5107 ± 3690	3300 ± 3008
S40531/01	GD 50	...	...	189.0	−40.1	5915	3675 ± 3675	1800 ± 1026	1246 ± 1142	2294 ± 1719	4199 ± 4199	3648 ± 3648
S40532/01	BD +532820	333.5	54.4	101.2	−1.7	12,077	1391 ± 911	2007 ± 1027	2051 ± 1025	4644 ± 1551	2624 ± 1612	3413 ± 2148
S40532/02	BD +532820	333.5	54.4	101.2	−1.7	6243	2872 ± 2872	2812 ± 1288	2370 ± 1105	3739 ± 2320	2063 ± 1241	3255 ± 2977
S40544/03	WD 0005+511	...	...	116.1	−10.9	2264	5746 ± 5746	3451 ± 1903	962 ± 962	2484 ± 2184	6321 ± 6321	2107 ± 2107
S40545/01	HD 36487	82.9	−7.1	210.2	−21.0	18,159	36,434 ± 1537	26,436 ± 608	23,044 ± 1264	20,756 ± 1465	18,531 ± 1191	21,654 ± 916
S40545/02	HD 36487	82.9	−7.1	210.2	−21.0	8461	35,871 ± 2674	25,708 ± 830	23,127 ± 1651	21,833 ± 1607	20,573 ± 1891	21,992 ± 1429
S40546/01	HD 36981	83.8	−5.2	208.8	−19.3	10565	293,331 ± 2799	282,397 ± 1501	387,482 ± 1565	441,446 ± 2536	447,431 ± 3448	423,016 ± 2065
S40546/02	HD 36981	83.8	−5.2	208.8	−19.3	5696	295,623 ± 4247	286,129 ± 1913	394,862 ± 1901	447,044 ± 2903	454,589 ± 3138	428,521 ± 2984
S40547/01	HD 72350	127.7	−44.7	262.7	−3.2	9375	12,257 ± 2641	15,741 ± 609	12,807 ± 1235	15,331 ± 1989	13,900 ± 1571	11,949 ± 1132
S40547/02	HD 72350	127.7	−44.7	262.7	−3.2	4283	12,018 ± 4164	16,791 ± 974	13,622 ± 2076	13,593 ± 2430	14,273 ± 2084	12,555 ± 1752
S40549/02	NCVZ	218.2	65.0	107.0	48.8	26,083	3191 ± 2670	1642 ± 552	1166 ± 605	2569 ± 1219	2150 ± 2150	2330 ± 2330
S40549/03	NCVZ	218.2	65.0	107.0	48.8	19,047	2720 ± 2486	1607 ± 653	1194 ± 848	2545 ± 1109	2880 ± 2880	2214 ± 1505

TABLE 2—*Continued*

Data Set	Target	R.A. (deg)	Decl. (deg)	l (deg)	b (deg)	Time (s)	1	2	3	4	5	6
S40550/01	Z-Cam	126.3	73.1	141.4	32.6	4497	4587 ± 3619	2042 ± 1238	823 ± 823	3391 ± 2426	1717 ± 1717	5073 ± 5073
S40553/01	WR 42-HD 97152	167.5	−61.0	290.9	−0.5	11,884	7747 ± 2859	5983 ± 792	8127 ± 1421	10,034 ± 1726	4936 ± 1401	5159 ± 1432
S40554/01	Sk −67D111	81.7	−67.5	277.8	−33.0	12,645	19,264 ± 2443	14,648 ± 742	12,697 ± 1036	14,773 ± 1808	29,656 ± 1614	28,805 ± 1153
S40555/01	PG 1520+525	230.5	52.4	85.4	52.4	7411	3620 ± 3620	2199 ± 1343	1011 ± 1011	2801 ± 1875	1449 ± 1449	901 ± 901
S40555/02	PG 1520+525	230.5	52.4	85.4	52.4	6183	4443 ± 3829	1216 ± 925	1022 ± 1022	3436 ± 2010	788 ± 788	1532 ± 1532
S40557/03	LSE 44	208.2	−48.1	313.4	13.5	3683	6048 ± 3058	4530 ± 1047	4423 ± 1313	4144 ± 1429	3613 ± 1826	3524 ± 1469
S40557/01	LSE 44	208.2	−48.1	313.4	13.5	18,164	8089 ± 1331	5533 ± 375	4756 ± 828	6296 ± 1176	4003 ± 834	3940 ± 643
S40557/02	LSE 44	208.2	−48.1	313.4	13.5	6238	7571 ± 2538	4847 ± 646	4100 ± 1152	5588 ± 1575	3979 ± 1429	3462 ± 758
S40557/04	LSE 44	208.2	−48.1	313.4	13.5	10,715	5084 ± 1571	5463 ± 591	4807 ± 835	5971 ± 1199	2787 ± 821	3085 ± 642
S40558/01	HD 102567	177.0	−62.2	295.6	−0.2	7395	8829 ± 4827	6690 ± 1181	6361 ± 1700	8071 ± 1857	7878 ± 1721	4706 ± 1389
S40563/01	WD 1634−573	249.6	−57.5	329.9	−7.0	15,616	4598 ± 3584	2873 ± 707	3452 ± 1069	4809 ± 1187	3172 ± 2104	1317 ± 866
S40563/02	WD 1634−573	249.6	−57.5	329.9	−7.0	2704	5337 ± 4845	4367 ± 2012	4355 ± 1746	4123 ± 2647	11832 ± 9902	4751 ± 4534
S40563/03	WD 1634−573	249.6	−57.5	329.9	−7.0	3422	5992 ± 5437	3615 ± 1101	4456 ± 2038	5645 ± 2422	4033 ± 4033	2432 ± 1850
S40563/04	WD 1634−573	249.6	−57.5	329.9	−7.0	12,029	6560 ± 4195	3468 ± 1154	2749 ± 907	3530 ± 1573	1888 ± 1138	1279 ± 1279
S40564/01	BD +43°4035	341.7	44.3	100.6	−13.1	5062	2584 ± 2584	2083 ± 1406	1277 ± 1277	2382 ± 2140	2873 ± 2643	1072 ± 940
S40573/01	HD 35580	80.6	−56.1	264.2	−34.5	10,555	3442 ± 3223	2571 ± 1094	1970 ± 1173	3236 ± 1075	2293 ± 2293	837 ± 837
S40573/01	HD 35580	80.6	−56.1	264.2	−34.5	10,555	4314 ± 3490	2529 ± 1029	2329 ± 1042	4088 ± 1463	2431 ± 1840	780 ± 780
S40578/01	HD 074,194	130.2	−45.1	264.0	−2.0	9611	11,045 ± 2313	20,502 ± 609	8553 ± 1394	8112 ± 2008	2395 ± 1157	1807 ± 675
S40584/01	WD 1725+586	261.7	58.6	87.2	33.8	3838	4191 ± 4191	2008 ± 1654	2631 ± 1613	3569 ± 2454	2623 ± 1330	950 ± 950
S40590/01	HE 2-138	237.9	−66.3	319.7	−9.5	10,839	2587 ± 2587	2749 ± 933	2664 ± 1154	3295 ± 1304	2217 ± 1648	2506 ± 1185
S40591/01	HD 104994	181.3	−62.1	297.6	0.3	3216	22,837 ± 7282	12,420 ± 1306	11,671 ± 2954	13,675 ± 3231	15,238 ± 2553	13,071 ± 2346

NOTES.—Cols. (1)–(6) give the surface brightness of the diffuse radiation observed in the respective rows of Table 1. The units are in photons cm^{-2} sr^{-1} s^{-1} $Å^{-1}$, and the uncertainties are 90% confidence limits.

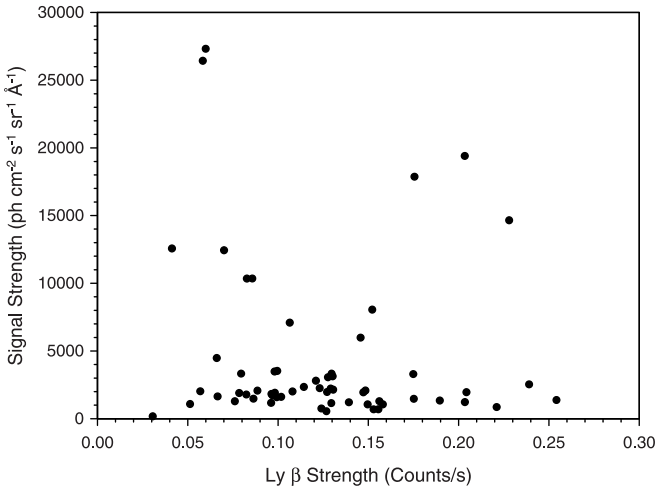

FIG. 3.—Derived diffuse continuum signal vs. total number of counts under the Lyβ line. If scattering from geocoronal Lyman lines is a significant contaminant of the observed spectrum, we would expect a correlation.

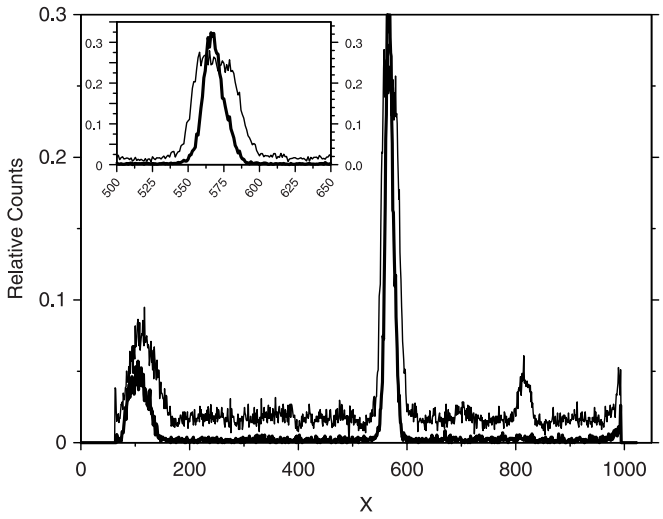

FIG. 4.—Vertical cut through the image showing that the point-spread function for a star (*lower line*) is much narrower than that for a diffuse source, in this case an observation in Orion. Note that the emission from the star is only visible in the LWRS, while the diffuse radiation is apparent in the LiF MDRS also. An expanded view of the profile in the vicinity of the LiF LWRS aperture is shown in the inset.

we have observed a diffuse astronomical signal are listed in Table 2. The sensitivity limit of the *FUSE* spectrographs to diffuse radiation is on the order of about 2000 photons cm^{-2} sr^{-1} s^{-1} Å^{-1}, and so the null detections are not interesting.

This procedure is tantamount to assuming that the instrumental background is the same in the aperture as off. There are several instrumental effects that may affect this, of which the most likely to be a problem is scattering in the spectral direction from the Lyman lines of atmospheric H I. We have tested for this by plotting the observed signal against the counts under the Lyβ line (Fig. 3) for a representative sample and found no correlation between the astronomical and geocoronal lines. While there are other possibilities, we have found no evidence for any aperture-dependent effects in our null detections—the signal is flat over the entire detector. Perhaps the strongest argument for the quality of our background subtraction comes from the excellent agreement between different segments and different observations, separated in time by as much as a year and a half, in all of which the derived background agrees within the error bars. The only exception is S4055401, in which the background derived from segment 2A is much higher than the others. An examination of the raw data shows that the count rate is much higher at the beginning of each exposure, suggesting contamination from daylight photons.

The signal levels are so low that stellar contamination might be a serious problem. The sensitivity limit of 2000 photons cm^{-2} sr^{-1} s^{-1} Å^{-1} corresponds to an unreddened B star of about 16th magnitude in *V*. We have examined each of the fields using the Digitized Sky Survey plates and have rejected those few fields in which there were stars that were bright enough to possibly affect our determination of the diffuse background. Most of these were in the SMC or LMC, where there are many hot bright stars, some of which did fall in the *FUSE* field of view. Another test of stellar contamination comes from the much broader spread for a diffuse source, which fills the aperture, as opposed to a point source (Fig. 4), and we have confirmed that the spread for those sources identified as diffuse is really larger than that for a star. In practice, there are few unreddened early-type stars in the sky, and any stellar contribution in the *FUSE* bandpass will be heavily depressed because of interstellar extinction. Finally, we excluded those observations in which the pointing was particularly poor.

We have also considered whether scattering from the nearby alignment star, which may be quite bright in the FUV, can contribute to the diffuse signal. The *FUSE* instrument team has studied the scattered light from γ Cas and found that the scattered light at a distance of 90″ from the star is on the order of 7×10^{-6} times the stellar flux (B.-G. Anderson 2003, private communication). Even the brightest stars in our sample, with an observed intensity of 10^{-11} ergs cm^{-2} sr^{-1} s^{-1}, will not contribute more than 200 photons cm^{-2} sr^{-1} s^{-1} Å^{-1} to the signal, much less than our sensitivity limit.

3. RESULTS

Of the 107 total observations (71 independent targets) in the S405/505 program (to our cutoff date), we have identified 45 (32 independent locations) as unquestionable detections of a diffuse astronomical signal. These positive detections are listed in Table 2 and range in strength from 1600 to a maximum of 3×10^5 photons cm^{-2} sr^{-1} s^{-1} Å^{-1} (in the Orion nebular region). The brightest of these are plotted in Figure 5 and show a variety of spectral shapes, perhaps indicative of the local radiation field. For instance, the scattered spectrum for S40546, a field in Orion, is very similar to that of the nearby star HD 36981 (J. Murthy et al. 2004, in preparation). We will discuss each of the individual regions in subsequent papers and concentrate on the global distribution of the diffuse background in this work. Images and further description of each of the fields may be found on the Web.[3]

There have been three studies of the UV/100 μm correlation in the near-UV. Haikala et al. (1995) found a ratio of 128 photons cm^{-2} sr^{-1} s^{-1} Å^{-1} (MJy sr^{-1})$^{-1}$ for an isolated cirrus cloud at high Galactic latitude using FAUST data, Schiminovich et al. (2001) found a latitude-dependent ratio of between 60 ($b > 30°$) and 100 ($b > 15°$) photons cm^{-2} sr^{-1} s^{-1} Å^{-1} (MJy sr^{-1})$^{-1}$ using the NUVIEWS instrument, and Murthy et al. (2001) found ratios varying between 30 and 300 photons cm^{-2}

[3] See http://www.iiap.res.in/personnel/murthy/projects/fuse/FUSE_background_analysis.html.

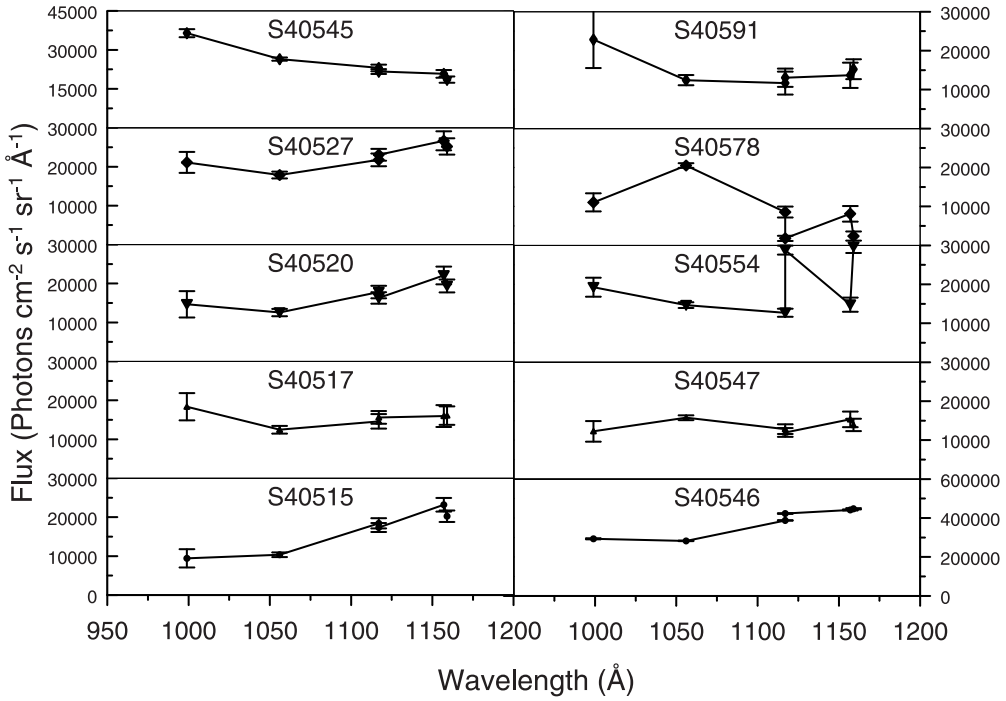

FIG. 5.—Flux extracted from each of the bands listed in Table 1 for each of the positive detections in our database. These include data from all the detectors except for 2B (for which the effective area was much less than for the other detectors). Note the generally excellent agreement in fluxes between different segments. The two brightest spectra (S40545 and S40546) are both of targets in Orion. Differences in the spectra may reflect different local radiation fields.

sr^{-1} s^{-1} $Å^{-1}$ (MJy sr^{-1})$^{-1}$ in *Midcourse Space Experiment* (*MSX*) observations around M42 in Orion. Our corresponding data are plotted in Figure 6 with the flux from the 1B spectrum at an effective wavelength of 1058 Å (mean wavelength for band 2 in Table 1) plotted against the 100 μm flux from Schlegel et al. (1998). Although there is a trend of increasing FUV emission with increasing IR, there is considerable variation in the ratio ranging from only 28 photons cm^{-2} sr^{-1} s^{-1} $Å^{-1}$ (MJy sr^{-1})$^{-1}$ near the Wolf-Rayet star HD 92809 (S40515)

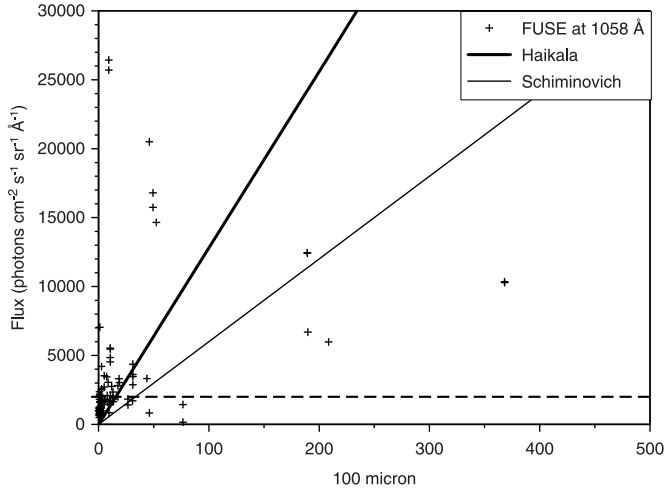

FIG. 6.—FUV/IR ratio showing a general trend of increasing FUV flux (at 1058 Å; Table 1, row [2]) with increasing 100 μm flux but with wide variations in the actual ratio. The two lines indicate the NUV/IR ratios obtained by Haikala et al. (1995) for an isolated high-latitude cirrus cloud (*thick line*) and by Schiminovich et al. (2001) for the high-latitude diffuse background. We have not plotted the brightest of our targets, S40546 in Orion, which has an observed surface brightness of 2.9×10^5 photons cm^{-2} sr^{-1} s^{-1} $Å^{-1}$ in the FUV and 2000 MJy sr^{-1} at 100 μm.

to 2800 photons cm^{-2} sr^{-1} s^{-1} $Å^{-1}$ (MJy sr^{-1})$^{-1}$ near the star HD 36487 in Orion (S40545). In fact, this variation should not be surprising. The UV signal arises from scattering of the interstellar radiation field (ISRF) by interstellar dust and so depends heavily on the relative orientation of the stars and the dust, particularly in the FUV where there are only a relatively small number of bright stars that dominate the ISRF. On the other hand, the IR emission is due to the thermal emission from the heated interstellar dust and is not dependent on the direction of the incoming radiation. Moreover, the optical depth in the UV is much higher than in the IR, and saturation effects may be expected to become important even with low column densities of dust.

As mentioned earlier, the only other major body of observations in the FUV is from observations made with the *Voyager* UVS (Murthy et al. 1999), and we have plotted those data as well as the data in this work in an Aitoff projection of the sky in Figure 7. In the figure, the area of the circles is proportional to the observed surface brightness with the large open circle in Orion corresponding to a surface brightness of 2.9×10^5 photons cm^{-2} sr^{-1} s^{-1} $Å^{-1}$. Note that we have not shown the *FUSE* null detections because the detection limit is too high to be useful. On the other hand, the *Voyager* null detections are at a level of only about 100 photons cm^{-2} sr^{-1} s^{-1} $Å^{-1}$ and are shown in the figure. Prominent hot spots in the map include Orion (near the right edge of Fig. 7; J. Murthy et al. 2004, in preparation), Ophiuchus (near $l = 0°$, $b = 28°$), and the Coalsack ($l = 305°$, $b = 0°$; Shalima & Murthy 2004), but it should also be noted that there are a number of dark regions even at low Galactic latitudes.

It is clear from the data presented in this paper that the intensity and the spectrum of the diffuse radiation in the FUV does vary considerably over the sky. Although other studies (see, e.g., Schiminovich et al. 2001 and references therein) have claimed simple correlations between the diffuse UV radiation and tracers of interstellar dust such as 21 cm H I column

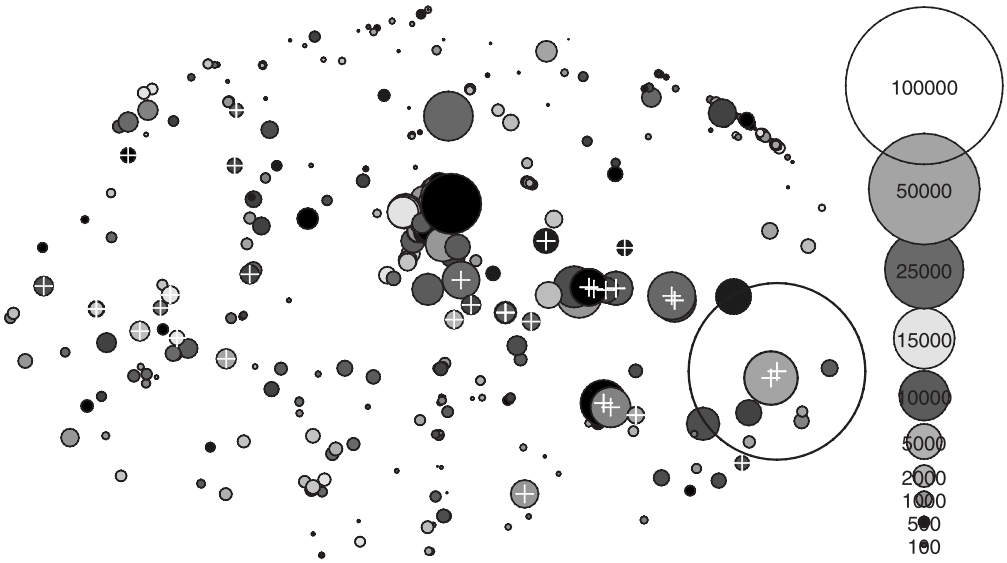

FIG. 7.—Combination of the 426 *Voyager* observations of Murthy et al. (1999) and the *FUSE* observations of this paper into an Aitoff projection of the diffuse FUV background with the Galactic center in the center of the image and $\pm 180^{\circ}$ at the left and right edges, respectively. The area of each circle is proportional to the observed surface brightness with the large open circle at the bottom right (Orion) having a brightness of 2.9×10^5 photons cm^{-2} sr^{-1} s^{-1} Å^{-1}. (Note that the colors are only for clarity and do not reflect the flux.) The circles with plus signs at the center are the *FUSE* observations presented in this paper, while the others are from Murthy et al. (1999). The brightest regions are Orion in the bottom right and Ophiuchus near the center. Note that we have not included the null detections of *FUSE* (those of less than about 2000 photons cm^{-2} sr^{-1} s^{-1} Å^{-1} in strength), which do not place useful limits on the diffuse signal. [*See the electronic edition of the Journal for a color version of this figure*.]

densities or 100 μm intensities in the NUV, we cannot support such claims from our data in the FUV. The optical depth of the interstellar dust is much higher in the FUV, and it is possible that local effects are more important than in the NUV. Thus we will defer modeling of our results to extract such important quantities as the optical properties of the interstellar dust grains.

4. CONCLUSION

We have used serendipitous observations of blank sky with the *FUSE* spacecraft to investigate the diffuse sky background in many areas over the sky. Of the total 71 independent pointings, we have observed a signal that we can unambiguously attribute to a diffuse background in 32 targets. Considering that the S405/505 targets were chosen simply on the basis of a nearby alignment star and considering that *FUSE* is only sensitive to signals of greater than 2000 photons cm^{-2} sr^{-1} s^{-1} Å^{-1}, this is a surprisingly large percentage. By contrast, in the *Voyager* sample of Murthy et al. (1999) only 63 of the total 426 targets have a flux of greater than 2000 photons cm^{-2} sr^{-1} s^{-1} Å^{-1}. Of course, in neither case was an unbiased survey of the diffuse radiation field intended, and it is likely that selection effects play an important role in these ratios.

We have found that there is a trend of increasing FUV flux with the 100 μm flux, indicating that the observed radiation is due to light scattered from the interstellar dust. However, the ratio between the FUV and the IR varies much more than was found by either Haikala et al. (1995) or Schiminovich et al. (2001) in the NUV. Our targets are in quite different locations in the sky, and it is apparent that local effects, such as exposure to the intense radiation field in Orion, play an important role in determining the scattering of the stellar radiation. Haikala et al. (1995) derived their ratio for a single isolated cirrus cloud, while Schiminovich et al. (2001) surveyed a large fraction of the sky.

If we combine our data with the *Voyager* data of Murthy et al. (1999), we see that the FUV sky is quite patchy with intensities ranging from upper limits of less than 100 photons cm^{-2} sr^{-1} s^{-1} Å^{-1} to intense regions as high as 3×10^5 photons cm^{-2} sr^{-1} s^{-1} Å^{-1}. These regions are scattered throughout the sky with both bright and faint regions being found at all latitudes, again suggesting that local effects dominate the FUV diffuse radiation field.

We thank the *FUSE* team for much helpful information and discussion. This research has made use of NASA's Astrophysics Data System and the SIMBAD database operated at CDS, Strasbourg, France. The data presented in this paper were obtained from the Multimission Archive at the Space Telescope Science Institute (MAST). STScI is operated by the Association of Universities for Research in Astronomy, Inc., under NASA contract NAS5-26555. Support for MAST for non-*HST* data is provided by the NASA Office of Space Science via grant NAG5-7584 and by other grants and contracts.

REFERENCES

Bowyer, S. 1991, ARA&A, 29, 59
Dixon, W. V. D., Kruk, J., & Murphy, E. 2002, The CalFUSE Pipeline Reference Guide (ver. 1.3; Baltimore: Johns Hopkins Univ.), http://fuse.pha.jhu.edu/analysis/pipeline_reference.html
Feldman, P. D., Sahnow, D. J., Kruk, J. W., Murphy, E. M., & Moos, H. W. 2001, J. Geophys. Res., 106, 8119
Haikala, L. K., Mattila, K., Bowyer, S., Sasseen, T. P., Lampton, M., & Knude, J. 1995, ApJ, 443, L33
Henry, R. C. 1991, ARA&A, 29, 89
Lampton, M., Margon, B., & Bowyer, S. 1976, ApJ, 208, 177
Moos, H. W., et al. 2000, ApJ, 538, L1
Murthy, J., Hall, D., Earl, M., Henry, R. C., & Holberg, J. B. 1999, ApJ, 522, 904

Murthy, J., Henry, R. C., Paxton, L. J., & Price, S. D. 2001, Bull. Astron. Soc. India, 29, 563
Sahnow, D. J., et al. 2000, Proc. SPIE, 4139, 131
Schiminovich, D., Friedman, P. G., Martin, C., & Morrissey, P. F. 2001, ApJ, 563, L161
Schlegel, D. J., Finkbeiner, D. P., & Davis, M. 1998, ApJ, 500, 525
Shalima, P., & Murthy, J. 2004, MNRAS, 352, 1319
Sodroski, T. J., Odegard, N., Arendt, R. G., Dwek, E., Weiland, J. L., Hauser, M. G., & Kelsall, T. 1997, ApJ, 480, 173